



Nuclear and Hybrid Equations of State in Light of the Low-Mass Compact Star in HESS J1731-347

L. Brodie ^{1,*} and A. Haber ^{1,†}

¹*Department of Physics, Washington University in St. Louis, St. Louis, MO 63130, USA*

(Dated: 3 February 2023)

We sample a wide range of relativistic mean-field theories (RMFTs) constrained by chiral effective field theory and properties of symmetric nuclear matter around saturation density and test them against known stellar structure constraints. This includes a relatively new mass and radius measurement of the central compact object in HESS J1731-347, which is reported to have an unusually low mass of $M = 0.77_{-0.17}^{+0.20} M_{\odot}$ and a compact radius of $R(1.4M_{\odot}) = 10.4_{-0.78}^{+0.86}$ km. We show that none of the sampled nuclear RMFTs meet all stellar structure constraints at the 68% credibility level, but that hybrid equations of state with a quark matter inner core and nuclear outer core fulfill all constraints at the 68% credibility level. This indicates a tension between astrophysical constraints and low-energy nuclear theory if future measurements confirm the central values reported above.

I. INTRODUCTION

Constraining the equation of state (EOS) of dense matter and the phase diagram of quantum chromodynamics (QCD) is one of the great tasks of modern theoretical physics [1–5]. By combining astrophysical observations with theoretical calculations, we can study the otherwise inaccessible high-density and low-temperature part of the QCD phase diagram. Each conjectured EOS has to be thoroughly tested against current astrophysical constraints [6–9] to validate its high-density behavior [10–16]. First principle calculations, chiral effective field theory (χ EFT) at low densities [17–20] and perturbative QCD at high densities [21–24], put additional constraints on the EOS. On the astrophysical side, stellar masses, radii and tidal deformabilities (which strongly depend on the compactness of a star, i.e. the ratio of mass and radius) play a major role in constraining the EOS, because they can be computed from the EOS directly by solving the Tolman-Oppenheimer-Volkoff equations from general relativity. In the last decade, compact stars with masses greater than two solar masses measured accurately via Shapiro delay [25–27] have ruled out many models. More recently, measurements of stellar radii [6, 8, 28, 29] have started to restrict the allowed mass-radius parameter space. In 2022, the central compact object (CCO) in HESS J1731-347 was reported to have a low mass of $M = 0.77_{-0.17}^{+0.20} M_{\odot}$ and compact radius of $R(1.4M_{\odot}) = 10.4_{-0.78}^{+0.86}$ km [9]. In this publication, we test how well models of nuclear matter describe known stellar structure constraints, including the CCO in HESS J1731-347. For this purpose, we sample hundreds of relativistic mean-field theories (RMFTs) constrained at low densities by χ EFT following the procedure we developed in Ref. [15]. RMFTs are useful tools that allow us to model nuclear matter across the wide range

of densities and temperatures found in neutron stars and their mergers [30–33]. Besides the EOS, RMFTs provide a consistent framework for chemical equilibration [34, 35], response to magnetic fields [36, 37], and calculations of transport properties such as bulk viscosity [38, 39]. After discussing traditional nuclear models, we show that hybrid stars with an inner core of quark matter and an outer core of nuclear matter can meet all astrophysical constraints at the 68% credibility level. To do so we combine a soft nuclear EOS, where the pressure does not rise rapidly with density leading to small stellar radii predictions, at low densities with a constant speed of sound model (CSS) for quark matter at high densities. We constrain the free parameters of the model using astrophysical constraints and show the compatibility of our results with other recent studies, for example a Bayesian analysis of the speed of sound in compact stars [40] or constraints from perturbative QCD [41, 42]. Our approach differs from the proposed solution of a strange quark star in Refs. [9, 43] because we study hybrid EOSs that model a nuclear matter phase below a critical transition density instead of postulating pure strange quark matter stars. A similar idea was presented in Ref. [44], where the authors focus on hybrid stars that form so-called “twin stars” [45–48], which achieve a small radius by branching off a stiffer nuclear EOS. Twin stars might be disfavored according to Ref. [14].

This paper is organized as follows: In Sec. II we investigate how the sampled RMFTs obey a wide range of astrophysical constraints including the mass and radius measurement of the CCO in HESS J1731-347 presented in Ref. [9]. In Sec. III we augment the RMFT with a phase transition to quark matter and show that these hybrid models are capable of reproducing all astrophysical measurements at the 68% credibility level, while the nuclear models are only compatible at the 95% credibility level. We end by presenting our conclusions in Sec. IV. In all our calculations we use natural units, $\hbar = c = k_B = 1$.

*Electronic address: b.liam@wustl.edu

†Electronic address: ahaber@physics.wustl.edu

II. NUCLEAR EQUATIONS OF STATE

In this section, we test how well nuclear EOSs can meet the following astrophysical constraints:

- The mass measurement of pulsar J0740+6620 from Ref. [6]: $M = (2.072 \pm 0.066) M_{\odot}$.
- The multimessenger constraints from Ref. [7] using the NICER+XMM-Newton result of Miller et al. [8], which combines NICER and XMM-Newton observations of pulsars, tidal deformability constraints from two gravitational-wave detections – GW170817 and GW190425, and detailed modeling of the kilonova AT2017gfo and the gamma-ray burst GRB170817A.
- The mass-radius measurement of the CCO in supernova remnant HESS J1731-347 reported in Ref. [9] with a low mass of $M = 0.77^{+0.20}_{-0.17} M_{\odot}$ and compact radius of $R = 10.4^{+0.86}_{-0.78}$ km.

We sample over 500 RMFTs within the χ EFT uncertainty band for pure neutron matter from Ref. [18] for densities between $0.5n_0$ and $1.5n_0$, where $n_0 = 0.16 \text{ fm}^{-3}$ is the saturation density of isospin-symmetric nuclear matter. This guarantees that our RMFTs do not violate the best available theoretical constraints for pure neutron matter at zero temperature (Fig. 1). We furthermore ensure that all sampled RMFTs reproduce known experimental and inferred properties of isospin-symmetric nuclear matter around saturation density [49–51], see [15] for more details. The sampled RMFTs have the same interaction terms as the well-established IU-FSU RMFT [52]. To test for model-induced biases we add additional meson self-interaction terms and re-fit the model to the pressure curve obtained without the additional interaction terms. We find variations smaller than the uncertainties introduced by χ EFT which lead to only minor changes in the mass-radius curve. Below a baryon density of $n_B \approx 0.25 n_0$ we attach the GPPVA(TM1e) crustal EOS from CompOSE [53]. This crustal EOS combines the Baym-Pethick-Sutherland EOS [54] for densities below $n_B = 0.002 \text{ fm}^{-3}$ with a Thomas-Fermi calculation [55] using the TM1e RMFT [56] for the inner crust. The complete sampling, crust attachment procedure, and Lagrangian can be found in Ref. [15]. Varying the crust transition density between $0.1n_0$ and $0.5n_0$ and using different crustal EOSs influences $R(1.4M_{\odot})$ and $R(0.7M_{\odot})$ on the order of $\Delta R \approx 100$ m and has no major influence on the conclusions presented in this work. Out of more than 500 RMFTs we sample, none of them obey all astrophysical constraints at the 68% credibility level and only 25 can fulfill the 95% credibility constraints (Fig. 2). Fig. 1 depicts the uncertainty band from χ EFT [18] (bounded by blue, dashed lines) of the binding energy of pure neutron matter, which can not be probed experimentally. While the orange lines show the entirety of our sampled models, the black solid

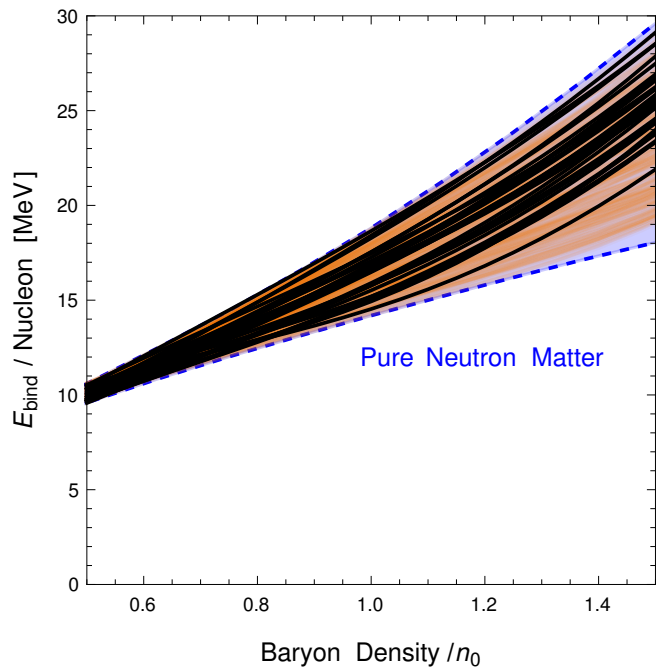


FIG. 1: Binding energy per nucleon as a function of baryon number density in pure neutron matter. The blue χ EFT uncertainty band is from Ref. [18]. We sample over 500 RMFTs (orange lines) in this uncertainty band and compute the corresponding mass-radius curves. The 25 samples that predict a maximum mass greater than two solar masses and go through all 95% credibility contours of the astrophysical constraints described at the beginning of Sec. II are shown in black.

lines represent the 25 models that are able to obey all astrophysical constraints described at the beginning of this section at the 95% credibility level. For an EOS to predict a star with a small radius of 10 – 11 km and mass of $M \approx 0.77 M_{\odot}$, the EOS must have small pressures at low densities. This implies a rather flat curve in the binding-energy band since the pressure can be obtained as a derivative of the binding energy with respect to the density. To meet the two solar mass constraint, the binding-energy curve must be as flat as possible and then rapidly increase, such that the pressure becomes large enough to sustain a two solar mass star. Even the most extreme RMFTs that we sampled were not able to achieve this and thereby fulfill all constraints at the 68% credibility level. For most of the models it is only the irregular shape of the mass-radius contour reported in Ref. [9] that allows them to meet all constraints at the 95% credibility level. We show this in Fig. 2, where we plot the mass-radius curves of the 25 “successful” models from our sampling procedure. The various shaded lines and contours depict the astrophysical constraints described at the beginning of this section. Should further measurements confirm the central value reported in Ref. [9], there will be a notable tension with low-energy nuclear physics computed from first principles via χ EFT, especially given that several χ EFT higher order calcula-

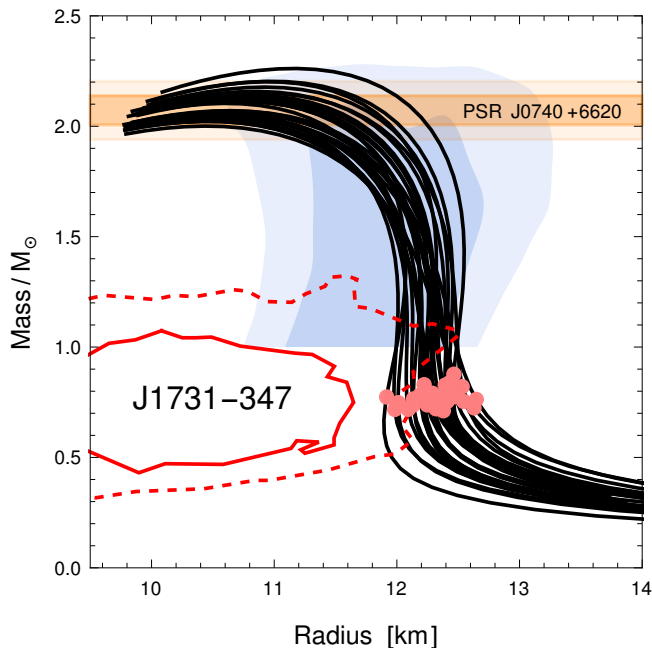


FIG. 2: Mass-radius curves for the RMFTs sampled in Fig. 1 that obey all relevant astrophysical constraints at the 95 % credibility level. The orange-shaded bars show the 68 % credibility (dark shading) and 95 % credibility (light shading) mass measurement of pulsar J0740+6620 from Ref. [6]. The blue shaded area shows the 68 % credibility (dark shading) and 95 % credibility (light shading) multimessenger constraints from Ref. [7] using the NICER+XMM-Newton result of Miller et al. [8]. The red solid(dashed) line shows the 68%(95 %) credibility mass-radius contours for the CCO in HESS J1731-347 from Ref. [9]. The pink dots indicate a central density of $n_B = 2n_0$, the uppermost density to which χ EFT might be reliable.

tions imply an even stiffer EOS at low densities [57, 58] than used here to constrain our models. This is further amplified by the pink dots in Fig. 2, which indicate a central density of $n_B = 2n_0$, the uppermost density to which χ EFT might be reliable [18, 20]. A star that light can therefore be completely described within χ EFT and does not require a high-density extension using RMFTs. In Ref. [9], the authors present various mass-radius curves extracted from the same χ EFT data shown in this publication that seemingly meet all observational constraints at the 68 % credibility level. These curves are not obtained using an RMFT but rather by extending a simple parametrization of the χ EFT band to higher densities [18]. Within our framework, we were not able to fit an RMFT to the corresponding curves shown in Ref. [9].

III. HYBRID EQUATIONS OF STATE

In this section, we show that augmenting the nuclear EOS with a first-order phase transition to quark matter allows us to accommodate all astrophysical constraints

at the 68 % credibility level. The mass-radius curve then contains a branch of hybrid stars with an inner core of quark matter and an outer core consisting of ordinary nuclear matter. To construct the hybrid EOS we use the constant speed of sound (CSS) model developed in Ref. [59]. We use this model to attach an EOS with a constant speed of sound to a nuclear EOS in a thermodynamically consistent way, i.e. we demand that pressure and baryon chemical potential vary smoothly across the phase transition and that the baryon density is a monotonically increasing function with respect to the baryon chemical potential. The energy density as a function of the pressure (i.e. the EOS) is given by

$$\varepsilon(P) = \begin{cases} \varepsilon_{\text{NM}}(P) & P \leq P_{\text{tr}} \\ \varepsilon_{\text{NM}}(P_{\text{tr}}) + \Delta\varepsilon + c_{\text{QM}}^{-2}(P - P_{\text{tr}}) & P \geq P_{\text{tr}} \end{cases}, \quad (1)$$

where $\varepsilon_{\text{NM}}(P)$ is the nuclear EOS. This EOS has three independent parameters, the transition pressure P_{tr} where the quark matter phase becomes energetically preferred, the jump in the energy density $\Delta\varepsilon$ which determines the strength of the first order phase transition and the (constant) speed of sound in the quark matter c_{QM} , which determines the stiffness of the quark part of the EOS. Although there are more sophisticated approaches to hybrid EOSs (see e.g. [60, 61]), our simple approach allows us to easily examine the parameter space and show how hybrid models can accommodate the low mass and radius measurement of the compact object in HESS J1731-347.

For the nuclear part of our hybrid EOS, we choose a rather soft nucleonic RMFT that we call QMC-Soft with a radius prediction $R = 11.47$ km at $M = 0.77 M_{\odot}$. QMC-Soft's coupling constants and nuclear matter properties can be found in Tab. I. For a detailed discussion of the couplings and the Lagrangian as well as all relevant thermodynamic quantities see Ref. [15]. We follow the same procedure for attaching a crustal EOS as described in Sec. II. The binding energy per nucleon for pure neutron matter and isospin-symmetric nuclear matter of the nucleonic EOS is shown in Fig. 3. The properties of isospin-symmetric nuclear matter at saturation density, e.g. the symmetry energy J and its slope L at saturation density are within experimental constraints, see e.g. Ref. [62]. Because the pressure from QMC-Soft does not rise rapidly as density increases, this nuclear EOS can not support a two solar mass neutron star, as shown in Fig. 4.

We vary the three parameters of the CSS EOS to study the possible astrophysical predictions and test them against all astrophysical constraints described at the beginning of Sec. II. For simplicity, we translate the transition pressure P_{tr} to the corresponding transition baryon density n_{tr} . The initial parameter range we consider is $n_{\text{tr}} \in [2n_0, 3n_0]$, $c_{\text{QM}}^2 \in [0.36, 1]$, and $\Delta\varepsilon/\varepsilon_{\text{tr}} \in [0.003, 0.84]$. We further restrict the parameter space by discarding all models that do not predict a two solar mass star or form a detached or unstable/non-existent hybrid branch. For a detailed mapping of the

Name	g_σ	g_ω	g_ρ	b	c	b_1	B	n_{sat}	$\mathcal{E}(n_{\text{sat}})$	$\kappa(n_{\text{sat}})$	J	L
Unit							[MeV ⁴]	[fm ⁻³]	[MeV]	[MeV]	[MeV]	[MeV]
QMC-Soft	6.58	6.56	10.87	0.0051	0.0949	13.357	-933761	0.158	-16.01	249	32.19	42.43

TABLE I: Couplings, pressure offset B , and selected properties for the QMC-Soft nuclear part of the hybrid EOS.

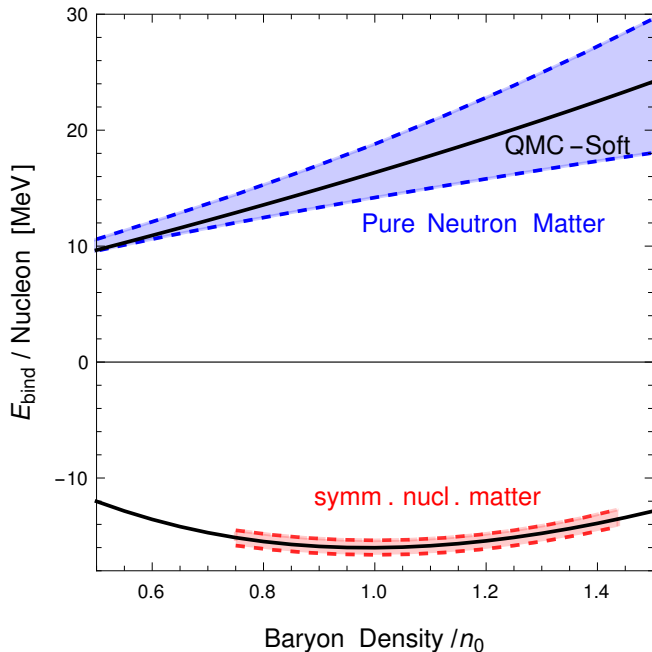


FIG. 3: Binding energy per nucleon as a function of baryon number density in pure neutron matter and isospin-symmetric nuclear matter. The blue dashed χ EFT uncertainty band is from Ref. [18]. The red dashed band represents a range of binding energies of isospin-symmetric nuclear matter using typical properties of nuclear matter, consistent with Refs. [49–51]. The solid lines represent the binding energy curves from the nuclear part of the hybrid EOS, termed QMC-Soft. The nuclear EOS agrees well with all known low-density experimental and theoretical constraints as shown in this plot and in Tab. I.

CSS parameter space see Ref. [59, 63]. The lowest speed of sound squared in our study that can sustain a heavy compact star is given by $c_{\text{QM}}^2 \approx 0.4$. Recent studies have shown that the speed of sound in heavy stars likely supersedes the conformal, high-density limit $c_{\text{conf.}}^2 = 1/3$, see for example Refs. [40, 64]. The bottom right panel of Fig. 2 within Ref. [40] indicates a nearly constant mean value for the speed of sound squared in the core of a two solar mass star around $c^2 \approx 0.4 - 0.5$. For simplicity, we fix the speed of sound squared to a value close to the radial average of the mean of the distribution in Ref. [40], $c_{\text{QM}}^2 = 0.48$ and explore the remaining parameter space. In Fig. 5 we plot the mass-radius curves predicted by our hybrid EOSs with $c_{\text{QM}}^2 = 0.48$ that match **all** astrophysical constraints described in Sec. II at the 68% credibility level. The transition densities (indicated by the gray dots) vary from $n_{\text{tr}} = 2n_0$ to $n_{\text{tr}} = 2.4n_0$ and the

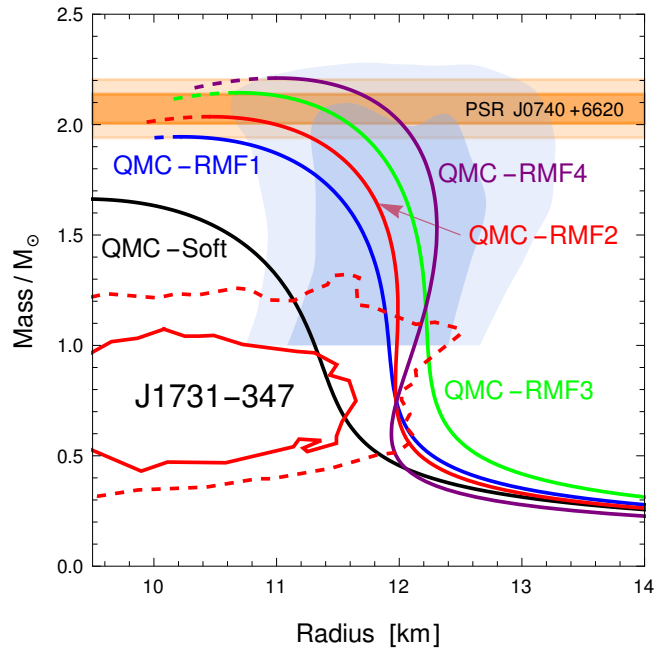


FIG. 4: Mass-radius curve of standard nucleonic stars predicted by QMC-Soft (defined in Tab. I and shown in black), which describes the nuclear outer core of our hybrid stars shown in Fig. 5. To accommodate the 68% credibility mass-radius constraints from Ref. [9] (solid red line), the pressure of the nuclear model cannot rise rapidly with density. QMC-Soft alone can therefore not sustain a two solar-mass compact star made of neutrons, protons, and electrons only. For comparison, we plot the nucleonic QMC-RMFs from Ref. [15]. All shaded contours are described in Fig. 2.

jump in the energy density varies from $\Delta\varepsilon/\varepsilon_{\text{tr}} \approx 0.004$ to $\Delta\varepsilon/\varepsilon_{\text{tr}} \approx 0.151$. We observe an inverse correlation between the transition density and the strength of the phase transition in the successful models: a higher transition density requires a smaller jump in the energy density (a weaker first-order phase transition) to obey all constraints. Otherwise, detached branches will form. We note that the speed of sound in quark matter or even in nuclear matter could be significantly higher, as shown in Ref. [40]. On average, the chosen value of $c_{\text{QM}}^2 = 0.48$ is certainly not unrealistic and a reasonable approximation to the EOS of quark matter, which is largely unknown. It is possible, however, to construct hybrid EOSs with a speed of sound as low as $c_{\text{QM}}^2 \approx 0.4$ that also obey all presented constraints at the 68% credibility level. The exact model parameters for all EOSs presented in Fig. 5 can be found online at gitlab.com/ahaber. This includes the dimensionless tidal deformabilities of a $M = 1.4 M_\odot$ star

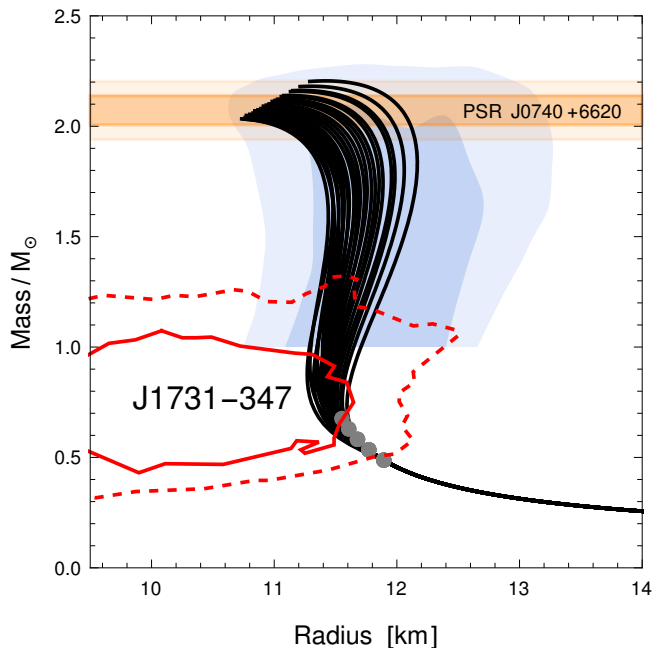


FIG. 5: Mass-radius curves of hybrid stars with $c_{\text{QM}}^2 = 0.48$ in the quark matter phase and an outer core described by QMC-Soft, the nuclear model in Fig. 3. The gray dots denote the transition point from the nuclear to the quark phase. All shaded contours are described in Fig. 2.

for all the presented models in Fig. 5, which range from $\Lambda_{1.4M_\odot} = 247$ to $\Lambda_{1.4M_\odot} = 391$ and are well within the observational constraints from Refs. [65–68]. We compute the dimensionless tidal deformability via the second tidal love number [69]. There are corrections to the second tidal love number in the presence of strong first-order phase transitions that affect the I-Love-Q relations (see Fig. 1 within Ref. [70]) at the level of a few percent [71–75]. Given that the hybrid models investigated in this paper show a rather weak first order phase transition and that the change in the dimensionless tidal deformability is well within known current constraints, we neglect these corrections. We furthermore verify the consistency of these hybrid EOSs with constraints from perturbative QCD as derived in Refs. [41, 42], using the code the authors of Ref. [42] provide publicly.

IV. CONCLUSIONS

We sample over 500 RMFTs constrained at low densities by χEFT and inferred properties of isospin-symmetric nuclear matter to study how well they obey astrophysical constraints. We notice that the new observation of a very light and compact star with $M = 0.77_{-0.17}^{+0.20} M_\odot$ and a radius of $R = 10.4_{-0.78}^{+0.86}$ km is barely compatible with our sampled RMFTs at the 95% credibility level if other well-established observational constraints are taken into account. We are not

able to construct an RMFT (within the chosen model parameter space) that obeys all constraints listed at the beginning of Sec. II at the 68% credibility level. If future measurements confirm the mean of the mass and radius and shrink the uncertainty, there will be tension between χEFT and astrophysical measurements. The core of neutron stars with $M \approx 0.77M_\odot$ can be completely described by χEFT limiting any uncertainties introduced by using RMFTs. In the second part of the paper we thus present an alternative solution: a hybrid star with an outer core of nuclear matter and an inner core of quark matter. We show that such hybrid models can easily meet all constraints at the 68% credibility level if the transition density from nuclear to quark matter takes place below $n_{\text{tr}} \approx 2.5n_0$ and does not require a strong first-order phase transition. To also support a heavy, two solar mass star, the speed of sound squared in quark matter has to be above $c_{\text{QM}}^2 \approx 0.4$. The radial dependence of the speed of sound in the entire star shows a nearly identical behavior as the mean of the Bayesian analysis presented in the bottom right panel of Fig. 2 in Ref. [40]: a nearly constant speed of sound in the inner part of the star (which we model with a quark matter EOS) and a rapid drop off in the outer regions (modeled with the nuclear QMC-Soft RMFT). As pointed out in Ref. [72], we want to emphasize that the existence of a quark matter core opens up the possibility of a softer nuclear EOS because the nuclear EOS does not have to support two solar mass compact stars.

Acknowledgements

We thank Mark G. Alford, Sophia Han, Ingo Tews, and Ziyuan Zhang for their input. This research was partly supported by the U.S. Department of Energy, Office of Science, Office of Nuclear Physics, under Award No. #DE-FG02-05ER41375.

-
- [1] S. Bogdanov et al. (2019), 1903.04648.
- [2] M. Maggiore et al., JCAP **03**, 050 (2020), 1912.02622.
- [3] M. Evans et al. (2021), 2109.09882.
- [4] A. Lovato et al. (2022), 2211.02224.
- [5] S. Bogdanov et al., in *2022 Snowmass Summer Study* (2022), 2209.07412.
- [6] T. E. Riley et al., *Astrophys. J. Lett.* **918**, L27 (2021), 2105.06980.
- [7] P. T. H. Pang, I. Tews, M. W. Coughlin, M. Bulla, C. Van Den Broeck, and T. Dietrich, *Astrophys. J.* **922**, 14 (2021), 2105.08688.
- [8] M. C. Miller et al., *Astrophys. J. Lett.* **918**, L28 (2021), 2105.06979.
- [9] V. Doroshenko, V. Suleimanov, G. Pühlhofer, and A. Santangelo, *Nature Astronomy* **6**, 1444 (2022).
- [10] R. Nandi, P. Char, and S. Pal, *Phys. Rev. C* **99**, 052802 (2019), 1809.07108.
- [11] R. Essick, I. Tews, P. Landry, S. Reddy, and D. E. Holz, *Phys. Rev. C* **102**, 055803 (2020), 2004.07744.
- [12] S. K. Greif, K. Hebeler, J. M. Lattimer, C. J. Pethick, and A. Schwenk, *Astrophys. J.* **901**, 155 (2020), 2005.14164.
- [13] G. Raaijmakers, S. K. Greif, K. Hebeler, T. Hinderer, S. Nissanke, A. Schwenk, T. E. Riley, A. L. Watts, J. M. Lattimer, and W. C. G. Ho, *Astrophys. J. Lett.* **918**, L29 (2021), 2105.06981.
- [14] I. Legred, K. Chatziioannou, R. Essick, S. Han, and P. Landry, *Phys. Rev. D* **104**, 063003 (2021), 2106.05313.
- [15] M. G. Alford, L. Brodie, A. Haber, and I. Tews, *Phys. Rev. C* **106**, 055804 (2022), 2205.10283.
- [16] M. Salinas and J. Piekarewicz (2023), 2301.09692.
- [17] J. E. Lynn, I. Tews, J. Carlson, S. Gandolfi, A. Gezerlis, K. E. Schmidt, and A. Schwenk, *Phys. Rev. Lett.* **116**, 062501 (2016), 1509.03470.
- [18] I. Tews, J. Carlson, S. Gandolfi, and S. Reddy, *Astrophys. J.* **860**, 149 (2018), 1801.01923.
- [19] D. Lonardonì, I. Tews, S. Gandolfi, and J. Carlson, *Phys. Rev. Res.* **2**, 022033(R) (2020), 1912.09411.
- [20] C. Drischler, J. A. Melendez, R. J. Furnstahl, and D. R. Phillips, *Phys. Rev. C* **102**, 054315 (2020), 2004.07805.
- [21] R. Somasundaram, I. Tews, and J. Margueron (2022), 2204.14039.
- [22] T. Gorda, K. Hebeler, A. Kurkela, A. Schwenk, and A. Vuorinen (2022), 2212.10576.
- [23] E. Annala, T. Gorda, A. Kurkela, J. Nättilä, and A. Vuorinen, *Nature Phys.* **16**, 907 (2020), 1903.09121.
- [24] E. Annala, T. Gorda, A. Kurkela, and A. Vuorinen, *Phys. Rev. Lett.* **120**, 172703 (2018), 1711.02644.
- [25] J. Antoniadis, P. C. Freire, N. Wex, T. M. Tauris, R. S. Lynch, et al., *Science* **340**, 6131 (2013), 1304.6875.
- [26] H. T. Cromartie et al., *Nature Astron.* **4**, 72 (2019), 1904.06759.
- [27] E. Fonseca et al., *Astrophys. J. Lett.* **915**, L12 (2021), 2104.00880.
- [28] M. C. Miller et al., *Astrophys. J. Lett.* **887**, L24 (2019), 1912.05705.
- [29] T. E. Riley et al., *Astrophys. J. Lett.* **887**, L21 (2019), 1912.05702.
- [30] J. D. Walecka, *Annals of Physics* **83**, 491 (1974).
- [31] J. Boguta and A. R. Bodmer, *Nucl. Phys. A* **292**, 413 (1977).
- [32] B. D. Serot and J. D. Walecka, *Adv. Nucl. Phys.* **16**, 1 (1986).
- [33] N. K. Glendenning, *Compact Stars* (Springer, 1996).
- [34] M. G. Alford, A. Haber, S. P. Harris, and Z. Zhang, *Universe* **7**, 399 (2021), 2108.03324.
- [35] E. R. Most, A. Haber, S. P. Harris, Z. Zhang, M. G. Alford, and J. Noronha (2022), 2207.00442.
- [36] A. Broderick, M. Prakash, and J. M. Lattimer, *Astrophys. J.* **537**, 351 (2000), astro-ph/0001537.
- [37] A. Haber, F. Preis, and A. Schmitt, *Phys. Rev. D* **90**, 125036 (2014), 1409.0425.
- [38] M. G. Alford and S. P. Harris, *Phys. Rev. C* **100**, 035803 (2019), 1907.03795.
- [39] M. Alford, A. Harutyunyan, and A. Sedrakian, *Phys. Rev. D* **100**, 103021 (2019), 1907.04192.
- [40] C. Ecker and L. Rezzolla, *Astrophys. J. Lett.* **939**, L35 (2022), 2207.04417.
- [41] O. Komoltsev and A. Kurkela (2021), 2111.05350.
- [42] T. Gorda, O. Komoltsev, and A. Kurkela (2022), 2204.11877.
- [43] F. Di Clemente, A. Drago, and G. Pagliara (2022), 2211.07485.
- [44] L. Tsouloukidis, P. S. Koliogiannis, A. Kanakis-Pegios, and C. C. Moustakidis, *Phys. Rev. D* **107**, 023012 (2023), 2210.15644.
- [45] N. K. Glendenning and C. Kettner, *Astron. Astrophys.* **353**, L9 (2000), astro-ph/9807155.
- [46] K. Schertler, C. Greiner, J. Schaffner-Bielich, and M. H. Thoma, *Nucl. Phys. A* **677**, 463 (2000), astro-ph/0001467.
- [47] J. J. Li, A. Sedrakian, and M. Alford, *Phys. Rev. D* **107**, 023018 (2023), 2207.09798.
- [48] J. J. Li, A. Sedrakian, and M. Alford (2023), 2301.10940.
- [49] H. A. Bethe, *Ann. Rev. Nucl. Part. Sci.* **21**, 93 (1971).
- [50] S. Shlomo, V. M. Kolomietz, and G. Colò, *European Physical Journal A* **30**, 23 (2006).
- [51] B.-A. Li, P. G. Krastev, D.-H. Wen, and N.-B. Zhang, *Eur. Phys. J. A* **55**, 117 (2019), 1905.13175.
- [52] F. J. Fattoyev, C. J. Horowitz, J. Piekarewicz, and G. Shen, *Phys. Rev. C* **82**, 055803 (2010), 1008.3030.
- [53] S. Typel, M. Oertel, and T. Klähn, *CompOSE CompStar online supernova equations of state harmonising the concert of nuclear physics and astrophysics*, URL <https://compose.obspm.fr/eos/207>.
- [54] G. Baym, C. Pethick, and P. Sutherland, *Astrophys. J.* **170**, 299 (1971).
- [55] F. Grill, H. Pais, C. Providência, I. Vidaña, and S. S. Avancini, *Phys. Rev. C* **90**, 045803 (2014), 1404.2753.
- [56] H. Shen, F. Ji, J. Hu, and K. Sumiyoshi, *Astrophys. J.* **891**, 148 (2020), 2001.10143.
- [57] C. Drischler, K. Hebeler, and A. Schwenk, *Phys. Rev. Lett.* **122**, 042501 (2019), 1710.08220.
- [58] M. Piarulli, I. Bombaci, D. Logoteta, A. Lovato, and R. B. Wiringa, *Phys. Rev. C* **101**, 045801 (2020), 1908.04426.
- [59] M. G. Alford, S. Han, and M. Prakash, *Phys. Rev. D* **88**, 083013 (2013), 1302.4732.
- [60] I. F. Ranea-Sandoval, S. Han, M. G. Orsaria, G. A. Contrera, F. Weber, and M. G. Alford, *Phys. Rev. C* **93**, 045812 (2016), 1512.09183.
- [61] E. S. Fraga, R. da Mata, S. Pitsinikos, and A. Schmitt,

- Phys. Rev. D **106**, 074018 (2022), 2206.09219.
- [62] C. Drischler, R. J. Furnstahl, J. A. Melendez, and D. R. Phillips, Phys. Rev. Lett. **125**, 202702 (2020), 2004.07232.
 - [63] C. Drischler, S. Han, J. M. Lattimer, M. Prakash, S. Reddy, and T. Zhao, Phys. Rev. C **103**, 045808 (2021), 2009.06441.
 - [64] S. Altiparmak, C. Ecker, and L. Rezzolla, Astrophys. J. Lett. **939**, L34 (2022), 2203.14974.
 - [65] B. P. Abbott et al. (LIGO Scientific, Virgo), Phys. Rev. Lett. **121**, 161101 (2018), 1805.11581.
 - [66] B. P. Abbott et al. (LIGO Scientific, Virgo), Phys. Rev. X **9**, 011001 (2019), 1805.11579.
 - [67] K. Chatziioannou, C.-J. Haster, and A. Zimmerman, Phys. Rev. D **97**, 104036 (2018), 1804.03221.
 - [68] K. Chatziioannou, Gen. Rel. Grav. **52**, 109 (2020), 2006.03168.
 - [69] T. Hinderer, Astrophys. J. **677**, 1216 (2008), 0711.2420.
 - [70] K. Yagi and N. Yunes, Phys. Rev. D **88**, 023009 (2013), 1303.1528.
 - [71] T. Damour and A. Nagar, Phys. Rev. D **80**, 084035 (2009), 0906.0096.
 - [72] V. Paschalidis, K. Yagi, D. Alvarez-Castillo, D. B. Blaschke, and A. Sedrakian, Phys. Rev. D **97**, 084038 (2018), 1712.00451.
 - [73] S. Han and A. W. Steiner, Phys. Rev. D **99**, 083014 (2019), 1810.10967.
 - [74] Z. Carson, K. Chatziioannou, C.-J. Haster, K. Yagi, and N. Yunes, Phys. Rev. D **99**, 083016 (2019), 1903.03909.
 - [75] J. Takátsy and P. Kovács, Phys. Rev. D **102**, 028501 (2020), 2007.01139.